Rapid Coeval Black Hole and Host Galaxy Growth in MRC 1138-262

Seymour, N.; Altieri, B.; De Breuck, C.; Barthel, P.; Coia, D.; Conversi, L.; Dannerbauer, H.; Dey, A.; Dickinson, M.; Drouart, G.

Published in:
Astrophysical Journal

DOI:
10.1088/0004-637X/755/2/146

The Astrophysical Journal, 755:146 (8pp), 2012 August 20 doi:10.1088/0004-637X/755/2/146

RAPID COEVAL BLACK HOLE AND HOST GALAXY GROWTH IN MRC 1138-262: THE HUNGRY SPIDER

N. Seymour[1,2], B. Altieri[3], C. De Breuck[4], P. Barthel[5], D. Coia[3], L. Conversi[3], H. Dannerbauer[6], A. Dey[7], M. Dickinson[7], G. Drouart[1,4,8], A. Galametz[9], T. R. Greve[10], M. Haas[11], N. Hatch[12], E. Ibar[13], R. Ivison[13,14], M. Jarvis[15,16], A. Kovács[17], J. Kurk[18], M. Lehnert[19], G. Miley[20], N. Nesvadba[19], J. I. Rawlings[2], A. Rettura[21], H. Röttgering[20], B. Rocca-Volmerange[8], M. Sánchez-Portal[3], J. S. Santos[3], D. Stern[21], J. Stevens[14], I. Valtchanov[3], J. Vernet[4], and D. Wylezalek[4]

[1] CSIRO Astronomy & Space Science, P.O. Box 76, Epping, NSW 1710, Australia
[2] Mullard Space Science Laboratory, University College London, Holmbury St Mary, Dorking, Surrey, RH5 6NT, UK
[3] Herschel Science Centre, European Space Astronomy Centre, ESA, Villanueva de al Cañada, E-28691 Madrid, Spain
[4] European Southern Observatory, Karl Schwarzschild Straße 2, D-85748 Garching, Germany
[5] Kapteyn Astronomical Institute, University of Groningen, P.O. Box 800, 9700-AV Groningen, The Netherlands
[6] Institut für Astrophysik, Universität Wien, Türkenschanzstraße 17, A-1180 Wien, Austria
[7] NOAO-Tucson, 950 North Cherry Avenue, Tucson, AZ 85719, USA
[8] Institut d Astrophysique de Paris, 98bis Bd Arago, F-75014 Paris, France
[9] INAF-Osservatorio di Roma, Via Frascati 33, I-00040, Monteporzio, Italy
[10] Department of Physics and Astronomy, University College London, Gower Street, London, WC1E 6BT, UK
[11] Astronomisches Institut, Ruhr-Universität Bochum, Universitätsstr. 150, Gebäude NA 7/173, D-44780 Bochum, Germany
[12] School of Physics and Astronomy, University of Nottingham, University Park, Nottingham, NG7 2RD, UK
[13] UK Astronomy Technology Centre, Royal Observatory, Blackford Hill, Edinburgh, EH9 3HJ, UK
[14] Institute for Astronomy, University of Edinburgh, Royal Observatory, Edinburgh, EH9 3HJ, UK
[15] Centre for Astrophysics Research, STRI, University of Hertfordshire, Hatfield, AL10 9AB, UK
[16] Physics Department, University of the Western Cape, Bellville 7535, South Africa
[17] Department of Astronomy, University of Minnesota, 116 Church St SE, Minneapolis, MN 55414, USA
[18] Max Planck Institut für extraterrestrische Physik, Postfach 1312, D-85741 Garching bei München, Germany
[19] GEPI, Observatoire de Paris, UMR 8111, CNRS, Université Paris Diderot, 5 place Jules Janssen, F-92190 Meudon, France
[20] Leiden Observatory, University of Leiden, P.O. Box 9513, 2300-RA Leiden, The Netherlands
[21] Jet Propulsion Laboratory, California Institute of Technology, Pasadena, CA 91109, USA
Received 2012 April 25; accepted 2012 June 22; published 2012 August 6

ABSTRACT

We present a detailed study of the infrared spectral energy distribution of the high-redshift radio galaxy MRC 1138-26 at $z = 2.156$, also known as the Spiderweb Galaxy. By combining photometry from *Spitzer*, *Herschel*, and LABOCA we fit the rest-frame 5–300 μm emission using a two-component, starburst, and active galactic nucleus (AGN) model. The total infrared (8–1000 μm) luminosity of this galaxy is $(1.97 \pm 0.28) \times 10^{13}\ L_{\odot}$ with (1.17 ± 0.27) and $(0.79 \pm 0.09) \times 10^{13}\ L_{\odot}$ due to the AGN and starburst components, respectively. The high derived AGN accretion rate of ~20% Eddington and the measured star formation rate (SFR) of $1390 \pm 150\ M_{\odot}\ \mathrm{yr}^{-1}$ suggest that this massive system is in a special phase of rapid central black hole *and* host galaxy growth, likely caused by a gas-rich merger in a dense environment. The accretion rate is sufficient to power both the jets and the previously observed large outflow. The high SFR and strong outflow suggest that this galaxy could potentially exhaust its fuel for stellar growth in a few tens of Myr, although the likely merger of the radio galaxy with nearby satellites suggests that bursts of star formation may recur again on timescales of several hundreds of Myr. The age of the radio lobes implies the jet started after the current burst of star formation, and therefore we are possibly witnessing the transition from a merger-induced starburst phase to a radio-loud AGN phase. We also note tentative evidence for [C II]158 μm emission. This paper marks the first results from the Herschel Galaxy Evolution Project (Project HeRGÉ), a systematic study of the evolutionary state of 71 high-redshift, $1 < z < 5.2$, radio galaxies.

Key words: galaxies: active – galaxies: formation – galaxies: high-redshift – galaxies: individual (MRC 1138-262)

1. INTRODUCTION

There is now a growing consensus that high-redshift radio galaxies (HzRG; $z > 1$, $L_{500\,\mathrm{MHz}} > 10^{26}\ \mathrm{WHz}^{-1}$) are markers of the early formation of the most massive galaxies, located within the highest peaks of dark matter overdensities (Miley & De Breuck 2008). Not only do HzRGs tend to reside in significantly overdense environments (e.g., Ivison et al. 2000; Stern et al. 2003; Venemans et al. 2007; Galametz et al. 2010, 2012; Tanaka et al. 2011; Mayo et al. 2012), but the mass of their stellar component also tends to be high as indicated by the remarkably tight scatter between the observed *K*-band magnitude and redshift (e.g., Lilly & Longair 1984; Eales et al. 1997; Jarvis et al. 2001; Willott et al. 2003; Rocca-Volmerange et al. 2004; Bryant et al. 2009). The high stellar masses have been confirmed more directly with rest-frame near-infrared observations (Seymour et al. 2007; De Breuck et al. 2010). Recent observations of the high mid-infrared luminosities of HzRGs indicate that the black holes in these sources likely have high accretion rates (Ogle et al. 2006; Seymour et al. 2007; Fernandes et al. 2011). HzRGs are often found with evidence of high star formation rates (SFRs) from detections in the submillimeter (e.g., Archibald et al. 2001; Stevens et al. 2003; Reuland et al. 2004), from their extended Lyα emission indicating large reservoirs of ionized gas (e.g., Reuland et al. 2003; Villar-Martín et al. 2003), from their CO emission indicating reservoirs of molecular H_2 (e.g., Papadopoulos et al. 2000; Emonts et al. 2011), from hot star ultraviolet absorption lines (e.g., Dey et al. 1997) and from their mid-infrared spectra (e.g., Seymour et al. 2008; Ogle et al.

2012). Kinematic measurements from ionized gas have also shown that HzRGs have extremely massive central black holes (3×10^9–2×10^{10} $M_\odot$; Nesvadba et al. 2011) consistent with the observed high stellar masses and accretion rates. All of these observations confirm the picture that HzRGs are markers of massive galaxies co-forming with a central black hole, residing in peaks of dark matter overdensity.

The exact formation mechanism of massive galaxies, and how the frequently observed radio-loud phase is related to black hole and galaxy growth, is often debated. A connection between the growth of the central black hole and the host galaxy has been proposed to reconcile semi-analytical models with observations. A form of "feedback," associated with a radio-loud phase, has been proposed to truncate the growth of the bulge and central black hole growth, thereby preventing the overproduction of massive galaxies being formed in these simulations (Bower et al. 2006; Croton et al. 2006). This idea has gained popularity with the kinematic observations suggesting powerful outflows from many HzRGs (e.g., Nesvadba et al. 2006), although most models favor scenarios where the winds are radiatively driven.

In order to test how phases of powerful radio-loud emission influence, or are associated with, the formation of massive galaxies at high-redshift, accurate measurements of the black hole accretion rate and the SFR are required. Due to varying, and difficult to determine, levels of obscuration at UV and optical wavelengths, as well as contamination from the active galactic nucleus (AGN), the best wavelength regime in which to obtain such measurements is the infrared (IR) where the spectral energy distributions (SEDs) of such sources also tend to peak. With the *Spitzer Space Telescope* (Werner et al. 2004) we conducted a systematic study with eight photometric bands (3.6–160 μm) of 71 HzRGs with redshifts, z, in the range $1 < z < 5.2$ in order to measure their near- to mid-IR rest-frame SEDs. This photometry allowed us to estimate separately the stellar and AGN contribution at these wavelengths, thereby confirming their high stellar masses and AGN mid-IR luminosities (Seymour et al. 2007; De Breuck et al. 2010). In order to measure the complete IR SED, we are now extending this study to far-IR wavelengths as the Herschel Radio Galaxy Evolution Project (Projet HeRGÉ). The *Herschel Space Telescope*[22] (Pilbratt et al. 2010) has already demonstrated that far-IR measurements can reliably be used to measure SFRs in powerful AGNs (e.g., Hardcastle et al. 2010; Hatziminaoglou et al. 2010; Shao et al. 2010; Seymour et al. 2011). By combining these data with those from *Spitzer* we can, for the first time, accurately measure the total bolometric luminosities and far-IR contribution, and then estimate the relative AGN and starburst IR luminosities in HzRGs.

In this paper we present the first results from Projet HeRGÉ on MRC 1138-262 at $z = 2.156$, otherwise known as the Spiderweb Galaxy due to the preponderance of satellite galaxies, "flies," revealed by deep *Hubble Space Telescope* (*HST*) imaging (Miley et al. 2006). This HzRG has a powerful AGN as implied by its high X-ray luminosity ($L_{2-10\,\mathrm{keV}} = 4 \times 10^{45}$ erg s^{-1} $\sim$ 1.0×10^{12} $L_\odot$; Carilli et al. 2002), its extreme radio emission ($L_{500\,\mathrm{MHz}} = 1.2 \times 10^{29}$ WHz^{-1}; De Breuck et al. 2010), and evidence of a high SFR ($\sim$1200 $M_\odot$ yr^{-1}; Stevens et al. 2003; Ogle et al. 2012). There is also evidence of a powerful outflow (Nesvadba et al. 2006) potentially driven by the massive central black hole (Nesvadba et al. 2011). A study of the proto-cluster environment of the Spiderweb Galaxy shows that many members will be stripped by, or merge with, the central galaxy by the present epoch (Hatch et al. 2009; Doherty et al. 2010; Tanaka et al. 2010). Kuiper et al. (2011) suggest that the measured dynamical structure around the Spiderweb Galaxy can be interpreted as the merger of two massive halos and that the combined system has not yet become virialized. In this paper we aim to measure more accurately the AGN accretion rate and SFR, the bolometrically dominant components, thereby obtaining an improved understanding of the evolutionary state of this HzRG.

In Section 2 we present the IR data used in this work and in Section 3 we present the SED fitting of these data with an AGN and starburst component. We discuss our results, and the overall evolutionary state of the Spiderweb Galaxy in Section 4 and conclude the paper in Section 5. Throughout this paper we use the "concordance" ΛCDM cosmology with $H_0 = 70$ Mpc^{-1} km s^{-1}, $\Omega_\Lambda = 1 - \Omega_M = 0.7$.

Table 1
Photometric Data

Wavelength (μm)	Flux Density (mJy)	Reference
24	3.89 ± 0.25	(1)
100	28.5 ± 3.1	(2)
160	43.0 ± 2.9	(2)
250	42.0 ± 7.2	(2)
350	38.9 ± 7.9	(2)
500	35.3 ± 8.3	(2)
870	6.7 ± 1.3	(3)

References. (1) De Breuck et al. 2010; (2) this work; (3) H. Dannerbauer et al. (2012, in preparation).

2. DATA

The data used in this work comprise observed infrared photometry across 20–1000 μm. At the shortest wavelength, 24 μm, the photometry comes from *Spitzer* and was published in De Breuck et al. (2010). We add additional contributions to the reported uncertainty, in quadrature, to allow for the absolute flux calibration and the color correction uncertainty as described in Seymour et al. (2007). We supplement this photometry with new observations from *Herschel* using the PACS (Poglitsch et al. 2010) and SPIRE (Griffin et al. 2010) instruments, as well as a LABOCA/870 μm flux density (H. Dannerbauer et al. 2012, in preparation, ESO program ID 084.A-1016(A) and MPG program ID 083.F-0022—both PI: J. Kurk). The *Herschel* observations were carried out as part of the project scientist guaranteed time (PI: Altieri).

The SPIRE observation (ObsID 1342210877) was performed using a four repetition cross-scan Large Map mode covering 10×10 arcmin, achieving 1σ instrumental noise of (3.5, 4.8, 5.4) mJy at (250, 250, 500 μm)—slightly below the SPIRE extragalactic confusion noise (Nguyen et al. 2010). To obtain SPIRE photometry for the Spiderweb Galaxy we used a time-line fitter,[23] which provides a better estimate of the flux density, because no binning into sky pixels is involved in the process. The final flux density uncertainty, reported in Table 1, includes the fit error, the confusion noise, and a conservative 7% flux calibration uncertainty (see the SPIRE Observers' Manual). The photometry from standard source fitting on maps is consistent

[22] *Herschel* is an ESA space observatory with science instruments provided by European-led Principal Investigator consortia and with important participation from NASA.

[23] The time-line fitter for SPIRE is available at the *Herschel*/SPIRE public Web site: herschel.esac.esa.int/twiki/bin/view/Public/SpireCalibrationWeb.

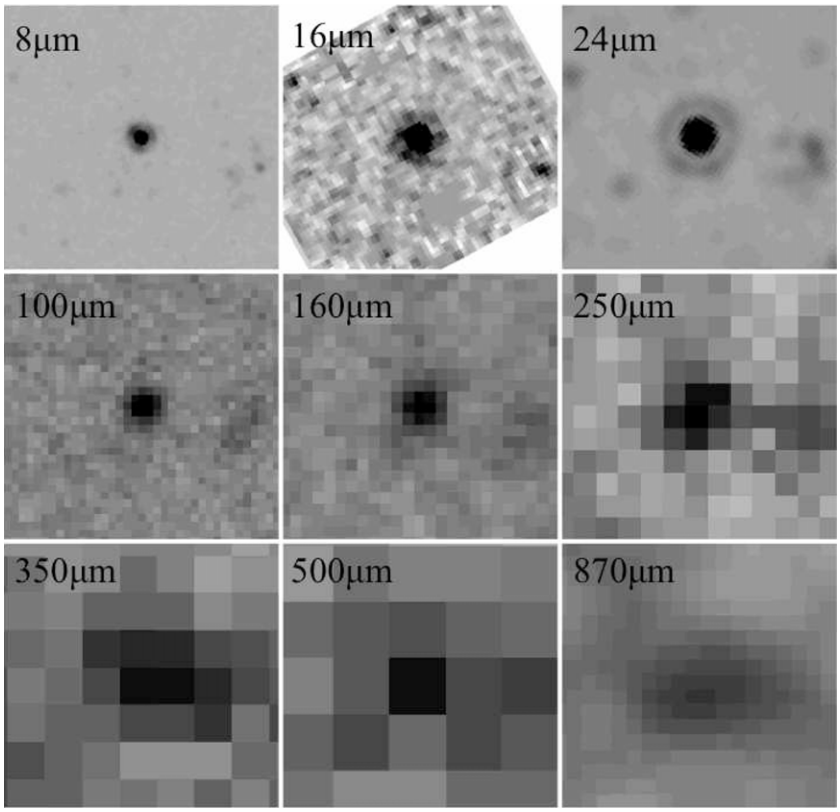

Figure 1. Postage-stamp IR images, 70 × 70 arcsec, of the Spiderweb Galaxy (R.A. 11:40:48.60, decl. −26:29:8.50; J2000) with north up and east to the left. From top left to bottom right the images are *Spitzer*/8/16/24 μm, PACS/100 and 160 μm, SPIRE 250/350/500 μm, and LABOCA/870 μm. The 8 and 16 μm bands are shown for illustration only and are not used in the model fitting. Note the Airy ring is quite prominent in the *Spitzer* data.

with the time-line fitter results, but we prefer to use the time-line fitter results as these are generally more accurate, especially for sources at high signal to noise. The PACS observations (ObsIDs 1342222456 and 1342222457) consisted of two crossed scan maps covering the same area and the data were reduced using HIPE v6.0 (Ott 2010). The data cubes were processed with a standard pipeline, including a sliding high-pass filtering on the detector time lines to remove detector drifts and $1/f$ noise with an iterative masking of the sources. We extracted flux densities via standard aperture photometry techniques and the PACS uncertainties include contributions from instrumental noise and absolute flux calibration. For the LABOCA/870 μm flux density uncertainty we add a 15% uncertainty, in quadrature, to the instrumental uncertainty to account for absolute flux calibration, atmospheric effects.

The *Herschel* beam varies from 6 to 36 arcsec, but the radio galaxy appears point like in all bands from 8 μm to 250 μm (see Figure 1). The 350, 500, and 870 μm images all show a slight extension in the east–west direction consistent with emission from the clump of galaxies approximately 30 arcsec to the west of the radio galaxy seen in the 8 μm through 250 μm bands. This extension is consistent with the SCUBA/850 μm detection by Stevens et al. (2003). This clump is comprised of four sources seen individually at 8 μm and 24 μm, the brightest two of which have been spectroscopically confirmed to lie at the same redshift and therefore be proto-cluster members (Kurk et al. 2004); hence, we can assume the long-wavelength flux density from these sources to have similar colors due to the Rayleigh–Jeans tail. We note the peak flux density at the longer wavelengths remains centered on the radio galaxy. We assume, for the purposes of SED fitting, that all this flux density comes from one source, but then treat the SFR measured from the starburst component as an upper limit to that from just the radio galaxy.

All the data used in the fitting of this sample are presented in Table 1.

3. SED FITTING

The goal of our SED fitting is to obtain the AGN and starburst IR luminosities (8–1000 μm) and then derive physical quantities from these results. We fit the observed photometry across 5–300 μm rest frame with a two-component model consisting of an AGN and a starburst template. Extrapolation of the radio core flux density using the observed flux densities at wavelengths $\geqslant$6 cm and the core spectral index from Carilli et al. (1997), $\alpha = -1.3$ ($S_\nu \propto \nu^\alpha$), suggests that synchrotron emission at these wavelengths is many orders of magnitude fainter. We use the `Decompir`[24] SED model fitting code (Mullaney et al. 2011) to fit the two components with some minor adaptations to use additional bandpass filters. The AGN component is an empirical model based on observations of moderate-luminosity (i.e., $L_{2-10\,\mathrm{keV}} = 10^{42}$–$10^{44}$ erg s^{-1}) low-redshift AGNs in Mullaney et al. (2011) selected at high X-ray energies from the local, $z < 0.1$, *Swift*-BAT sample (Tueller et al. 2008). This model is a continuous function comprised of two power laws and a modified blackbody, expressed as

$$F_\nu \propto \begin{cases} \lambda^{1.8} & \text{at} \quad 6\,\mu\mathrm{m} < \lambda < 19\,\mu\mathrm{m} \\ \lambda^{0.2} & \text{at} \quad 19\,\mu\mathrm{m} < \lambda < 40\,\mu\mathrm{m} \\ \nu^{1.5} F_\nu^{\mathrm{BB}} & \text{at} \quad \lambda > 40\,\mu\mathrm{m} \end{cases} . \qquad (1)$$

[24] http://sites.google.com/site/decompir/

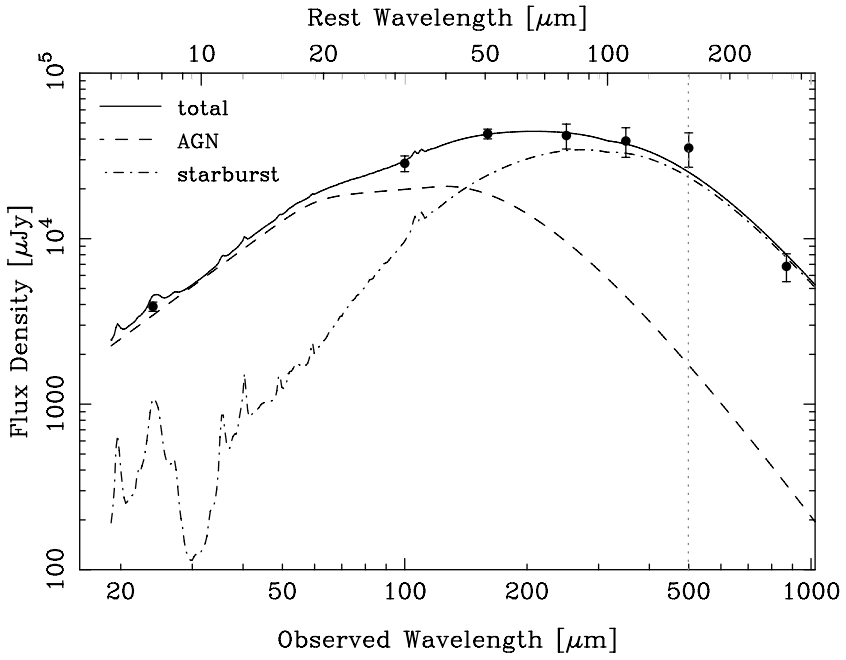

Figure 2. SED fit to the rest-frame 5–300 μm rest-frame photometry (black dots) of the Spiderweb Galaxy at $z = 2.156$ (MRC1138-262). The total model fit, AGN, and starburst components are indicated in the figure. The vertical gray dotted line represents the position of the [C II]158 μm line.

In comparison with other AGN templates commonly used, it is broadly similar in the mid-IR regime; however it has lower far-IR emission, when normalized at 19 μm, compared to NGC 1068 and Mrk 231, likely attributable to unaccounted starburst contributions at far-IR wavelengths in these two galaxies (Le Floc'h et al. 2001). This model is also broadly similar to empirical models presented by Richards et al. (2006) and Netzer et al. (2007). The advantage of the formulation above is that the various parameters (the two power-law slopes and the blackbody peak wavelength) can be adjusted to closely match these other models which we test later on.

The starburst models consist of five SEDs developed by Mullaney et al. from Brandl et al. (2006) designed to represent a typical range of SED types (i.e., peaking at a range of wavelengths). Beyond 100 μm these templates are extrapolated using a gray body with a frequency-dependent emissivity approximated as $\sim\nu^{\beta}$ with $\beta = 1.5$. In addition to the normalization and choice of starburst template, `Decompir` can apply extinction to each component separately. As the AGN-dominated mid-IR spectrum (Ogle et al. 2012) shows a little silicate emission, not absorption, we only allow the starburst component to be affected by absorption.[25] Therefore the chi-squared, χ^2, minimization performed by `Decompir` has four free components: normalization of each template, choice of starburst template and starburst extinction.

The best-fit combination of models returns a reduced chi-squared of $\chi^2_r = 1.4$ with the starburst template, "SB4," the template peaking at the shortest wavelength. We note that while the best-fit model has some extinction for the starburst component, it is poorly constrained and we get an equally good fit with no extinction and similar luminosities within 2%. The fit is shown in Figure 2 and the luminosities are reported in Table 2. The model fits the data well, although at the longest wavelengths the model slightly struggles to fit the sharp decrease in flux density from 500 to 870 μm. The SED at these wavelengths is dominated by the Rayleigh–Jeans tail of the starburst component and any blackbody would struggle to fit such a flux density ratio, although the slope does depend on the emissivity index. The "SB4" starburst template is the hottest of the five used,

Table 2
Derived Physical Properties

Property	Value	Reference
$L_{\rm IR}$(total)	$1.97 \pm 0.28 \times 10^{13}\ L_{\odot}$	(1)
$L_{\rm IR}$(AGN)	$1.17 \pm 0.27 \times 10^{13}\ L_{\odot}$	(1)
$L_{\rm IR}$(SB)	$0.79 \pm 0.09 \times 10^{13}\ L_{\odot}$	(1)
$M_{\rm gal}$ (stellar)	$\lesssim 1.1 \times 10^{12}\ M_{\odot}$	(2)
$M_{\rm BH}$	$\sim 1 \times 10^{10}\ M_{\odot}$	(3)
SFR (optical)	$57 \pm 8\ M_{\odot}\ {\rm yr}^{-1}$	(2)
Inclination, θ	$\leqslant 68^{\circ}$	(4)
Angular size	15.8 arcsec	(5)
$L_{2-10\,{\rm keV}}$ (unob.)	$< 1.0 \times 10^{12}\ L_{\odot}$	(6)
$L_{\rm BOL}$(AGN)	$\sim 7.0 \times 10^{13}\ L_{\odot}$	(1)
$R_{\rm Edd}$	~ 0.2	(1)
SFR	$1390 \pm 150\ M_{\odot}\ {\rm yr}^{-1}$	(1)
sSFR	$\gtrsim 1.3\ {\rm Gyr}^{-1}$	(1)
$t_{\rm char}$	$\lesssim 0.8$ Gyr	(1)
$D/\sin(\theta)$	~ 140 kpc	(1)
$L_{151\,{\rm MHz}}$	$5.6 \times 10^{29}\ {\rm WHz}^{-1}$	(1)
$L_{1\,{\rm keV}}$ (lobe)	$(1.8–4.5) \times 10^{11}\ L_{\odot}$	(1)
$t_{\rm jet}$	5–25 Myr	(1)

Notes. Results of SED fitting are listed first, parameters from the literature are listed second, and derived measurements in this work are listed last. Total IR luminosities are integrated over 8–1000 μm. SFR is based on the Kennicutt (1998) conversion which uses a Salpeter IMF.

References. (1) This work; (2) Hatch et al. (2009)—note the SFR is integrated over a 32 kpc radius; (3) Nesvadba et al. 2011; (4) G. Drouart et al. (2012, submitted); (5) Carilli et al. 1997; (6) Carilli et al. 2002.

[25] We note that while the X-ray emission from the AGN shows moderate extinction, $N_H = (2.6 \pm 0.6) \times 10^{22}$ cm^{-2} (Carilli et al. 2002), the mid-IR SED does not (Ogle et al. 2012). This is consistent with the bright Hα seen by Nesvadba et al. (2006) and can be attributed to differences in dust grains seen toward the circumnuclear regions of AGNs and the diffuse interstellar medium of our Galaxy.

with a dust temperature of $T_{\rm dust} \sim 64$ K. The next two cooler templates, $T_{\rm dust} \sim 46$–53 K, give a $\chi_r^2 \approx 5$–8 and fit the 500 μm flux density better, but exceed the 870 μm flux density by $\geqslant 4\sigma$.

If we exclude the 500 μm data point we marginally improve the best fit to $\chi_r^2 = 1.1$, again for the "SB4" template and with the output parameters changing very little (note the number of degrees of freedom drops by one). One potential method to better fit the observed high 500–870 μm flux ratio is to use starburst SEDs with a steeper emissivity index. By modifying the templates so that $\beta = 2$ we can obtain a steeper slope on the Rayleigh–Jeans side of the SED peak. Repeating the SED fitting with these modified starburst templates we obtain a best fit of $\chi_r^2 = 1.1$ from the modified "SB5" starburst template. The overall fit does not significantly change with a slightly smaller 500 μm excess, by ~20%, as well as an AGN luminosity increase of ~10% and a starburst luminosity decrease of ~20%. Hence, there is no significant improvement with this change to the starburst templates.

Visual examination of the images at 350, 500, and 870 μm, see Figure 1, suggests the measured flux densities at these wavelengths may have contributions from other proto-cluster members as discussed in Section 2. As the galaxies responsible for this emission lie at the same redshift, and are almost certainly starbursts to be emitting at these wavelengths, they likely have similar flux density ratios. The 250 μm flux density is not affected by these nearby sources and the peak flux density still originates from the central radio galaxy. The ratio of the radio galaxy to companion peak flux densities at 250 μm is about 2:1; hence, we estimate the contribution of the companion to the measured flux density at longer wavelengths to be ~1/3 at most. We note that the 350 μm flux density need only be decreased by 25% to produce an unphysical flux density ratio for a cold dust SED. However, if we decrease the three longest wavelength flux densities by this much the best fit gives a starburst luminosity only 10% lower. Hence, although the estimated starburst IR luminosity is formally an upper limit for the radio galaxy, we postulate that the true starburst IR luminosity of the Spiderweb Galaxy is, at most, only 10% lower.

We do not have enough photometry at $5\,\mu{\rm m} \leqslant \lambda_{\rm rest} \leqslant 50\,\mu$m to allow all the AGN parameters (the two power-law slopes and the blackbody peak), other than the normalization, to vary simultaneously. Allowing just one parameter to vary results in changes of luminosities of <5%. We can change the parameters in Equation (1) to mimic the Richards et al. (2006) and Netzer et al. (2007) AGN models. In both cases, the AGN luminosity halves and the starburst luminosity doubles, but the fit is worse with $\chi_r^2 \sim 8.5$. We note that this fit is improved if we use the Richards or Netzer AGN model with the $\beta = 2$ starburst SED, with the same qualitative results, but with a $\chi_r^2 = 3.3$. We also tried using the suite of empirical starburst templates from Rieke et al. (2009) instead of the Brandl templates. The best-fit templates were also those peaking at the shortest wavelengths, i.e., the ultraluminous IR galaxy templates, but with a slightly higher chi-squared: $\chi_r^2 \sim 3$. To obtain a better understanding of the uncertainties we also randomly varied the flux densities with a Gaussian distribution based on their quoted uncertainties one hundred times and repeated the fitting procedures. We found the variance of the resulting luminosities to be $\leqslant$10%, i.e., less than the quoted uncertainties in Table 2.

We finish this section by noting that while there are many ways to tweak both the AGN and starburst templates and change the parameters of the fit all solutions have an AGN component dominating at the shortest wavelengths, $\lambda_{\rm rest} \leqslant 30\,\mu$m, and a starburst component dominating at long wavelengths $\lambda_{\rm rest} \geqslant 60\,\mu$m. Hence, all good fits have a powerful, $L_{\rm IR}$ (SB/AGN) $> 5 \times 10^{12}\,L_\odot$, starburst, and AGN component. Until we get high spatial and/or spectral resolution data, e.g., from ALMA or *James Webb Space Telescope*, it will be difficult to differentiate between many moderately good fits.

4. DISCUSSION

We have measured very high AGN and starburst luminosities which imply a high central black hole accretion rate and SFR, respectively. The total IR luminosity of this system causes it to be classed as a hyper-luminous IR galaxy, $L_{\rm IR} > 10^{13}\,L_\odot$. We discuss here what these results mean and how they relate to the radio emission and overall evolutionary state of the system. We also discuss the potential origin of the 500 μm excess.

4.1. AGN Power

The total IR AGN luminosity marks the Spiderweb Galaxy as one of the most powerful AGNs known; therefore the AGN is likely having a strong effect on its host galaxy and immediate environment (see Section 4.6). Assuming the full unobscured AGN SED is similar to the Elvis et al. (1994) templates, we get $L_{\rm BOL}({\rm AGN}) \sim 6 \times L_{\rm IR}({\rm AGN})$ (we note other unobscured AGN templates produce similar numbers) and therefore an AGN bolometric luminosity of $\sim 7 \times 10^{13}\,L_\odot$. This bolometric AGN luminosity estimate is higher than previous estimates, e.g., Nesvadba et al. (2006) who used the observed X-ray luminosity (Carilli et al. 2002) and corrected it using the Elvis et al. (1994) template, $L_{\rm BOL}({\rm AGN}) \sim 10 \times L_{2-10\,{\rm keV}}({\rm AGN})$.

This discrepancy is unlikely due to extinction as seen toward the nucleus in X-rays given the low absorbing column (Carilli et al. 2002). As noted earlier, neither the mid-IR spectrum (Ogle et al. 2012) nor the SED (G. Drouart et al. 2012, submitted) indicates significant extinction either. The discrepancy between the hard X-ray and IR-derived bolometric AGN luminosities is more likely due to the dispersion between individual sources and the Elvis et al. (1994) templates. This, in turn, could be explained by a different dust-to-gas ratio in this source, a clumpy torus or an unusual AGN geometry, but further investigation is beyond the scope of this paper.

This galaxy exhibits both a large-scale central velocity distribution indicative of a powerful outflow (Nesvadba et al. 2006) and a high-luminosity mid-IR H_2 molecular emission line (Ogle et al. 2012). The derived bolometric radiative power would therefore be enough to power both the outflow ($\sim 8 \times 10^{12}\,L_\odot$; Nesvadba et al. 2006) and the probably shock-heated gas ($\sim 4 \times 10^{10}\,L_\odot$; Ogle et al. 2012), even assuming a 10% coupling efficiency. However, the kinetic power of the radio jet, estimated to be (0.6–8.0) $\times 10^{13}\,L_\odot$ by Nesvadba et al. (2011), is also powerful enough to potentially drive the outflow.

Nesvadba et al. (2006) also present an estimate of the black hole mass from the measurement of the central Hα luminosity and FWHM. The principle uncertainty in this measurement is how the orientation of the galaxy affects the application of the Greene & Ho (2005) scaling relationship, which is based on a sample of lower luminosity AGNs likely to be more face-on than the Spiderweb Galaxy, i.e., at lower inclinations. Indeed, G. Drouart et al. (2012, submitted) find a correlation between radio core prominence and viewing angle from a hot torus model fitted to the mid-IR SED of HzRGs which suggests that the radio axis is aligned to torus axis. These authors find that the Spiderweb Galaxy is inclined at angle of ~68° to

the line of sight, but has modest extinction, an $A_V \sim 1.5$. While generally there may be misalignments of up to 10°–20° between the radio and torus axes, it is likely that the Spiderweb Galaxy is more edge-on than the Greene & Ho (2005) sample. McLure & Dunlop (2002) show that the measured FWHM from a thin accretion disk is proportional to the sine of the inclination angle squared. Therefore, if the Spiderweb Galaxy has a higher inclination angle, $\theta_{\rm RG}$, than the mean value for the AGN sample used in Greene & Ho (2005), $\theta_{\rm GH05}$, then we would be overestimating the black hole mass by $\sin^2(\theta_{\rm GH05})/\sin^2(\theta_{\rm RG})$ which Nesvadba et al. (2011) assume to be ∼2. We therefore take the lower, inclination-corrected, value of the black hole mass from Nesvadba et al. (2011), $\sim 10^{10}\,M_\odot$. The higher bolometric luminosity derived above implies a higher black hole mass derived from the Hα luminosity. However, we also note the black hole mass reported here would put this galaxy on par with some of the most massive black holes known in the local universe (McConnell et al. 2011), and are very rare for the $z > 1$ universe. Hence, we treat this black hole mass as uncertain by a factor 2–3.

We then relate the bolometric luminosity to the maximally possible accretion luminosity where the continuum radiation force outward balances the gravitational force inward in hydrostatic equilibrium, i.e., the Eddington luminosity, and we find an Eddington accretion rate of ∼20%. This is a factor of a few higher than the estimate of Nesvadba et al. (2011) due to the higher bolometric luminosity and lower black hole mass used in this work. This high rate of accretion is common in less bolometrically luminous AGNs (∼25%; Kollmeier et al. 2006), but is rare for less radio-luminous AGNs ($L_{500\,\rm MHz} \lessapprox 10^{27}$ WHz^{-1}; Best & Heckman 2012) at least in the local, $z < 0.1$, universe. However, it is probably common for HzRGs as based on their X-ray (Overzier et al. 2005) and mid-IR (Ogle et al. 2006; Seymour et al. 2007) luminosities. These results suggest the accretion disk is in an efficient state, although the large outflow hints that it may soon run out of fuel.

4.2. Star Formation Rate

The starburst IR luminosity implies an SFR of $1390 \pm 150\,M_\odot$ yr^{-1} using the Kennicutt (1998) scaling relation (and therefore a Salpeter initial mass function, IMF). We noted in Section 2 that the longer wavelength bands may have some contribution from nearby proto-cluster members, but estimate that this contribution is ⩽10% in Section 3. This SFR is much higher than estimates from optical/near-IR data (Hatch et al. 2008, 2009), likely due to obscuration by dust, but is broadly consistent with estimates from the polycyclic aromatic hydrocarbon luminosities measured from the mid-IR SED (Ogle et al. 2012; J. Rawlings 2012, submitted). We note that the IR luminosity is more sensitive to the star formation averaged over a slightly longer time frame than optical/UV observations. We can estimate the mechanical energy of this starburst using the canonical conversion factor from Dalla Vecchia & Schaye (2008) and obtain a value $(1–2) \times 10^{11}\,L_\odot$ which is insufficient to explain the kinematics and outflow observed (Nesvadba et al. 2006). However, any material driven out may fall back onto the central galaxy or the satellite galaxies over time (e.g., Hatch et al. 2009, and see Section 4.6).

Estimating the stellar mass of this source is difficult due to the strong AGN continuum. Hatch et al. (2009) provide an estimate of $(1.1 \pm 0.2) \times 10^{12}\,M_\odot$ using SED fitting of high-resolution *HST* rest-frame UV/optical data. This result is consistent with the upper limit found from rest-frame near-IR observations (Seymour et al. 2007; De Breuck et al. 2010). We adopt the Hatch et al. (2009) value as an upper limit since it may still be contaminated by the AGN as it lies in the AGN-dominated region of mid-IR color–color space as shown in De Breuck et al. (2010). We can now derive the specific SFR, sSFR = SFR/$M_{\rm stellar}$, and find a value of $\gtrsim$1.3 Gyr^{-1}. This is a high sSFR, but common for star-forming galaxies at this redshift (Noeske et al. 2007; Elbaz et al. 2011). However, it is unusual for a galaxy this massive.

The inverse of the sSFR gives the characteristic time, $t_{\rm char}$, in which the galaxy would double its stellar mass if it maintains the current SFR. While this time frame is short, $\lesssim$0.8 Gyr, for the Spiderweb, it is likely that the star formation will turn off on even shorter timescales. Measurements of CO provide the best estimates of the mass of molecular hydrogen, i.e., the main component of the fuel for star formation and black hole growth (e.g., Emonts et al. 2011). While such measurements do not currently exist for the Spiderweb Galaxy we infer a value of $M_{\rm H_2} \sim (0.5–5) \times 10^{10}\,M_\odot$ based on the far-IR luminosity and the conversion factors used in Emonts et al. (2011) assuming the Spiderweb is similar to the HzRGs in that study. If we assume 100% star formation efficiency, then this SFR can only be maintained for another 4–40 Myr, neglecting infall from satellite galaxies which may happen within a few hundred Myr (see below). If the mass of material estimated to being removed by the outflow, $\gtrsim 400\,M_\odot$ yr^{-1} (Nesvadba et al. 2006), is taken into account, this time frame decreases by ∼30%, more if the powerful jets also entrain and remove significant amounts of gas from the galaxy, or if the molecular hydrogen mass is lower than assumed. If we assume a much lower star formation efficiency, e.g., 10%, then this timescale increases by an order of magnitude, but leaves fuel for further bursts of star formation triggered by its proto-cluster environment.

4.3. Age of Radio Jet

Previously, Nesvadba et al. (2006) estimated the age of the radio jet using the method put forth by Wan et al. (2000) and obtained a value of 4–10 Myr. We can re-estimate the age using models of radio lobe evolution from Mocz et al. (2011). These authors reproduce the emission at radio wavelengths from synchrotron processes and the X-rays emitted by the lobes due to inverse Compton (IC) scattering of the cosmic microwave background. These models lead to tracks of lobe radio/151 MHz and X-ray/1 keV luminosity against time and size of radio lobes at different redshifts. Carilli et al. (2002) estimate that 10%–25% of the X-ray emission they measure is spatially extended on scales of 10–20 arcsec, similar to the extent of the radio jet, 15.8 arcsec (Carilli et al. 1997). Hence, if we assume all this X-ray luminosity is from IC processes we get a lobe X-ray luminosity of $L_{2-10\,\rm keV} \sim (1–2.5) \times 10^{11}\,L_\odot$. As Mocz et al. (2011) use a 1 keV X-ray luminosity we take $L_{1\,\rm keV} \sim (1.8–4.5) \times 10^{11}\,L_\odot$ (assuming a photon power-law index of $\Gamma = 1.4$), and from the 365 and 74 MHz radio flux densities (Douglas et al. 1996; Cohen et al. 2007) we find a 151 MHz luminosity of $L_{151} = 5.6 \times 10^{29}$ WHz^{-1} $\sim 2.2 \times 10^{11}\,L_\odot$. Using the redshift and inclination estimate from G. Drouart et al. (2012, submitted) we estimate the total lobe size to be ∼140 kpc, which implies an age of ∼5 Myr in Figure 1 of Mocz et al. (2011) using the more powerful, $z = 2$ AGN track. Using the radio and X-ray luminosities, where $L_{151} \geqslant L_{1\,\rm keV}$, in Figure 3 of Mocz et al., we obtain an estimate of ⩽25 Myr for the age of the lobe. Hence, we take the age of the lobes to be in the range 5–25 Myr.

4.4. Possible [C II]158 μm Line

In Section 3 we reported an excess of emission in the 500 μm band which we measure to be 10.0 mJy at $\geqslant 1\sigma$ significance ($\sim 2\sigma$ just based on the instrumental noise). A potential explanation for this slight excess could be a significant contribution from the redshifted [C II]158 μm line ($\lambda_{\rm obs} = 499\,\mu$m). We note that no other lines, e.g., CO, fall within the 500 μm band width. Smail et al. (2011) examine the effect of strong far-IR emission lines on broadband photometry and show that such emission lines can cause measurable excesses in the broadband photometry. The excess measured here, 40% above the 25.3 mJy of the model, corresponds to a value of $L_{\rm [C\,II]}/L_{\rm IR} \sim 2.7\%$ (e.g., Figure 4 of Smail et al. 2011). While this value is higher, by a factor of $\sim$2, than any known value, it potentially indicates evidence for strong [C II]158 μm distributed across the proto-cluster environment, due to the extended 350–870 μm emission in the direction of confirmed proto-cluster members. The idea of a high, extended [C II] luminosity is consistent with the idea of a gaseous environment of neutral gas, ionized gas (Kurk et al. 2003), shocked H_2 (Ogle et al. 2012) and intra-galaxy star formation (Hatch et al. 2009) within this proto-cluster environment. We caution that the statistical significance of this result is poor but the Spiderweb Galaxy remains a promising target for far-IR/millimeter spectroscopy.

4.5. Evolutionary State of the Spiderweb Galaxy

We have determined that the Spiderweb Galaxy is in a rare, short-lived, phase of extreme, concurrent black hole, and host galaxy growth. If we compare the relative luminosities of the AGN and starburst component to the "continuous growth" relation in Lutz et al. (2010), i.e., the ratio required to maintain a constant black hole to stellar mass ratio, we see that the black hole is growing at a relatively faster rate by almost 1 dex. This result is consistent with the observed, albeit rather uncertain, ratio of stellar to black hole mass, $\leqslant$110, i.e., the black hole is relatively more massive (and has been growing rapidly) than it would be for the Spiderweb Galaxy to lie on the local "M–σ" mass ratio of $\sim$200 (Magorrian et al. 1998). The stellar and black hole masses do lie on the relationship found by Häring & Rix (2004) and we note that both observed relations have a large scatter, 0.3 dex. If this source is to end up on the local "M–σ" relation, further build-up of stellar mass is required. However, we have estimated that the SFR will likely rapidly decrease on timescales of $\sim$40 Myr assuming no further source of fuel.

Page et al. (2012) have recently examined the *Herschel*/250 μm detection rate of X-ray luminous AGNs in the Chandra Deep Field North in the $1 < z < 3$ redshift range as a function of X-ray luminosity. Those authors found that the fraction of X-ray AGNs detected with $S_{250\,\mu\rm m} \geqslant 18$ mJy decreases to zero above $L_{2-8\,\rm keV} = 10^{44}$ erg s^{-1} ($= 3 \times 10^{10}\,L_\odot$) and interpreted this result as suppression of star formation by powerful outflows driven by the AGN. The Spiderweb is a clear counter-example of this result with an X-ray luminosity well above this limit *and* a bright 250 μm detection, $S_{250} = 42$ mJy. However, Page et al. (2012) surveyed a small area, covering just 0.12 deg^2, and hence only probed a small volume where galaxies as massive as the Spiderweb are rare over this volume (e.g., Fontana et al. 2006). We can estimate an upper limit to the duty cycle of a simultaneous AGN and starburst activity above these limits by dividing the look-back time probed across $1 < z < 3$, 3.64 Gyr, by the number of X-ray AGNs in this study, 21, and obtain a value of 170 Myr. If the Spiderweb Galaxy is in a transition from merger-induced starburst phase to an AGN phase, and this transition is relatively short, <170 Myr, as the analysis here suggests, then the Page et al. (2012) results are consistent with our observations. We point out that such comparison is only valid if there are similar evolutionary processes going on in the less massive Page et al. (2012) sample.

4.6. Proto-cluster Environment

The environment of the Spiderweb Galaxy has been extensively studied and a full review of work in this area is beyond the scope of this paper. We have noted previously that this galaxy hosts one of the most powerful AGNs known: both from its bolometric luminosity (indicative of radiative power) and its radio luminosity (indicative of kinetic power). Tanaka et al. (2010) compared massive galaxies in the environment of the Spiderweb Galaxy with identically selected field galaxies from the GOODS-S field. They determined that the galaxies in the proto-cluster environment had formed earlier and had lower SFRs, particularly close to the HzRG and along the east–west distribution of proto-cluster members. The radio emission has the same projected east–west axes; hence, it is possible that the lower SFRs observed could be due to the influence of the AGN jet. Alternatively, they may simply be more heavily obscured.

As the Spiderweb Galaxy is situated in a well-studied proto-cluster we can estimate its future growth. Several authors have identified proto-cluster members and estimated that they would merge with, or be tidally stripped by, the radio galaxy before the present epoch. Hatch et al. (2009) identified 18 proto-cluster members through *HST* imaging within 150 kpc of the central radio galaxy, the combined mass of which they estimated to be $1.9^{+1.5}_{-0.8} \times 10^{11}\,M_\odot$. Doherty et al. (2010) spectroscopically confirmed two red galaxies within $\sim$500 kpc,[26] in addition to those mentioned above, with stellar masses of the order (3–5) $\times\ 10^{11}\,M_\odot$ each. Hence, the total stellar mass increase of the Spiderweb Galaxy over the upcoming $\sim$10 Gyr would be $\sim 10^{12}\,M_\odot$, i.e., at least a doubling in its mass, which would put it closer to the local "M–σ" relation. Kuiper et al. (2011) interpret their kinematic study of the environment, which showed a double-peaked velocity distribution, as being due the merger of two massive clusters. If each cluster contained a dominant central galaxy then the high AGN and starburst luminosities could well be due to a gas-rich merger of two large galaxies.

5. CONCLUSIONS

We have measured the total IR rest-frame SED of the Spiderweb Galaxy, for the first time, and fitted an AGN and starburst model components. We find that the bolometric luminosity of the AGN component of this source implies that the AGN has an accretion rate high enough to power both the jets and the observed outflow. The Spiderweb Galaxy has a high SFR; however, we estimate this SFR cannot be maintained for long and cannot be responsible for the outflow. We estimate the radio jets are 5–25 Myr old. At the current SFR, the host galaxy has only had enough time to accumulate $\sim$6% of its observed stellar mass while the jets were on. Hence, the jets were likely triggered after most of the current burst of star formation commenced. The central black hole is possibly growing at a relatively faster rate than the host galaxy (assuming this system will end up on the local M–σ relation). Studies of the proto-cluster environment

[26] Not the $\sim$300 kpc previously reported.

suggest that mergers of satellites, and hence increased star formation, will occur on timescales of hundreds of Myr and ultimately the stellar mass will double by the present epoch. We also see very tentative evidence for strong [C II]158 μm emission.

N.S. is the recipient of an Australian Research Council Future Fellowship. T.R.G. acknowledges support from the Science and Technologies Facilities Council, as well as IDA and DARK. We thank J. Mullaney for help using the DecompIR code. This work is based in part on observations made with the *Spitzer Space Telescope*, which is operated by the Jet Propulsion Laboratory, California Institute of Technology under a contract with NASA. Support for this work was provided by NASA through an award issued by JPL/Caltech. HIPE is a joint development by the Herschel Science Ground Segment Consortium, consisting of ESA, the NASA Herschel Science Center, and the HIFI, PACS, and SPIRE consortia

Facilities: Spitzer, *Herschel*, APEX

REFERENCES

Archibald, E. N., Dunlop, J. S., Hughes, D. H., et al. 2001, MNRAS, 323, 417
Best, P. N., & Heckman, T. M. 2012, MNRAS, 421, 1569
Bower, R. G., Benson, A. J., Malbon, R., et al. 2006, MNRAS, 370, 645
Brandl, B. R., Bernard-Salas, J., Spoon, H. W. W., et al. 2006, ApJ, 653, 1129
Bryant, J. J., Johnston, H. M., Broderick, J. W., et al. 2009, MNRAS, 395, 1099
Carilli, C. L., Harris, D. E., Pentericci, L., et al. 2002, ApJ, 567, 781
Carilli, C. L., Röttgering, H. J. A., van Ojik, R., Miley, G. K., & van Breugel, W. J. M. 1997, ApJS, 109, 1
Cohen, A. S., Lane, W. M., Cotton, W. D., et al. 2007, AJ, 134, 1245
Croton, D. J., Springel, V., White, S. D. M., et al. 2006, MNRAS, 365, 11
Dalla Vecchia, C., & Schaye, J. 2008, MNRAS, 387, 1431
De Breuck, C., Seymour, N., Stern, D., et al. 2010, ApJ, 725, 36
Dey, A., van Breugel, W., Vacca, W. D., & Antonucci, R. 1997, ApJ, 490, 698
Doherty, M., Tanaka, M., De Breuck, C., et al. 2010, A&A, 509, A83
Douglas, J. N., Bash, F. N., Bozyan, F. A., Torrence, G. W., & Wolfe, C. 1996, AJ, 111, 1945
Eales, S., Rawlings, S., Law-Green, D., Cotter, G., & Lacy, M. 1997, MNRAS, 291, 593
Elbaz, D., Dickinson, M., Hwang, H. S., et al. 2011, A&A, 533, A119
Elvis, M., Wilkes, B. J., McDowell, J. C., et al. 1994, ApJS, 95, 1
Emonts, B. H. C., Feain, I., Mao, M. Y., et al. 2011, ApJ, 734, L25
Fernandes, C. A. C., Jarvis, M. J., Rawlings, S., et al. 2011, MNRAS, 411, 1909
Fontana, A., Salimbeni, S., Grazian, A., et al. 2006, A&A, 459, 745
Galametz, A., Stern, D., De Breuck, C., et al. 2012, ApJ, 749, 169
Galametz, A., Vernet, J., De Breuck, C., et al. 2010, A&A, 522, A58
Greene, J. E., & Ho, L. C. 2005, ApJ, 630, 122
Griffin, M. J., Abergel, A., Abreu, A., et al. 2010, A&A, 518, L3
Hardcastle, M. J., Virdee, J. S., Jarvis, M. J., et al. 2010, MNRAS, 409, 122
Häring, N., & Rix, H.-W. 2004, ApJ, 604, L89
Hatch, N. A., Overzier, R. A., Kurk, J. D., et al. 2009, MNRAS, 395, 114
Hatch, N. A., Overzier, R. A., Röttgering, H. J. A., Kurk, J. D., & Miley, G. K. 2008, MNRAS, 383, 931
Hatziminaoglou, E., Omont, A., Stevens, J. A., et al. 2010, A&A, 518, L33
Ivison, R. J., Dunlop, J. S., Smail, I., et al. 2000, ApJ, 542, 27
Jarvis, M. J., Rawlings, S., Eales, S., et al. 2001, MNRAS, 326, 1585
Kennicutt, R. C. 1998, ARA&A, 36, 189
Kollmeier, J. A., Onken, C. A., Kochanek, C. S., et al. 2006, ApJ, 648, 128
Kuiper, E., Hatch, N. A., Miley, G. K., et al. 2011, MNRAS, 415, 2245
Kurk, J. D., Pentericci, L., Overzier, R. A., Röttgering, H. J. A., & Miley, G. K. 2004, A&A, 428, 817
Kurk, J., Röttgering, H., Pentericci, L., Miley, G., & Overzier, R. 2003, Nature, 47, 339
Le Floc'h, E., Mirabel, I. F., Laurent, O., et al. 2001, A&A, 367, 487
Lilly, S. J., & Longair, M. S. 1984, MNRAS, 211, 833
Lutz, D., Mainieri, V., Rafferty, D., et al. 2010, ApJ, 712, 1287
Magorrian, J., Tremaine, S., Richstone, D., et al. 1998, AJ, 115, 2285
Mayo, J. H., Vernet, J., De Breuck, C., et al. 2012, A&A, 539, A33
McConnell, N. J., Ma, C.-P., Gebhardt, K., et al. 2011, Nature, 480, 215
McLure, R. J., & Dunlop, J. S. 2002, MNRAS, 331, 795
Miley, G., & De Breuck, C. 2008, A&AR, 15, 67
Miley, G. K., Overzier, R. A., Zirm, A. W., et al. 2006, ApJ, 650, L29
Mocz, P., Lee, J. C., Iwasawa, K., & Canizares, C. R. 2011, ApJ, 729, 30
Mullaney, J. R., Alexander, D. M., Goulding, A. D., & Hickox, R. C. 2011, MNRAS, 414, 1082
Nesvadba, N. P. H., De Breuck, C., Lehnert, M. D., et al. 2011, A&A, 525, A43
Nesvadba, N. P. H., Lehnert, M. D., Eisenhauer, F., et al. 2006, ApJ, 650, 693
Netzer, H., Lutz, D., Schweitzer, M., et al. 2007, ApJ, 666, 806
Nguyen, H. T., Schulz, B., Levenson, L., et al. 2010, A&A, 518, L5
Noeske, K. G., Weiner, B. J., Faber, S. M., et al. 2007, ApJ, 660, L43
Ogle, P., Davies, J. E., Appleton, P. N., et al. 2012, ApJ, 751, 13
Ogle, P., Whysong, D., & Antonucci, R. 2006, ApJ, 647, 161
Ott, S. 2010, in ASP Conf. Ser. 434, Astronomical Data Analysis Software and Systems XIX, ed. Y. Mizumoto, K.-I. Morita, & M. Ohishi (San Francisco, CA: ASP), 139
Overzier, R. A., Harris, D. E., Carilli, C. L., et al. 2005, A&A, 433, 87
Page, M. J., Symeonidis, M., Vieira, J. D., et al. 2012, Nature, 485, 213
Papadopoulos, P. P., Röttgering, H. J. A., van der Werf, P. P., et al. 2000, ApJ, 528, 626
Pilbratt, G. L., Riedinger, J. R., Passvogel, T., et al. 2010, A&A, 518, L1
Poglitsch, A., Waelkens, C., Geis, N., et al. 2010, A&A, 518, L2
Reuland, M., Röttgering, H., van Breugel, W., & De Breuck, C. 2004, MNRAS, 353, 377
Reuland, M., van Breugel, W., Röttgering, H., et al. 2003, ApJ, 592, 755
Richards, G. T., Lacy, M., Storrie-Lombardi, L. J., et al. 2006, ApJS, 166, 470
Rieke, G. H., Alonso-Herrero, A., Weiner, B. J., et al. 2009, ApJ, 692, 556
Rocca-Volmerange, B., Le Borgne, D., De Breuck, C., Fioc, M., & Moy, E. 2004, A&A, 415, 931
Seymour, N., Ogle, P., De Breuck, C., et al. 2008, ApJ, 681, L1
Seymour, N., Stern, D., De Breuck, C., et al. 2007, ApJS, 171, 353
Seymour, N., Symeonidis, M., Page, M. J., et al. 2011, MNRAS, 413, 1777
Shao, L., Lutz, D., Nordon, R., et al. 2010, A&A, 518, L26
Smail, I., Swinbank, A. M., Ivison, R. J., & Ibar, E. 2011, MNRAS, 414, L95
Stern, D., Holden, B., Stanford, S. A., & Spinrad, H. 2003, AJ, 125, 2759
Stevens, J. A., Ivison, R. J., Dunlop, J. S., et al. 2003, Nature, 425, 264
Tanaka, I., Breuck, C. D., Kurk, J. D., et al. 2011, PASJ, 63, 415
Tanaka, M., De Breuck, C., Venemans, B., & Kurk, J. 2010, A&A, 518, A18
Tueller, J., Mushotzky, R. F., Barthelmy, S., et al. 2008, ApJ, 681, 113
Venemans, B. P., Röttgering, H. J. A., Miley, G. K., et al. 2007, A&A, 461, 823
Villar-Martín, M., Vernet, J., di Serego Alighieri, S., et al. 2003, MNRAS, 346, 273
Wan, L., Daly, R. A., & Guerra, E. J. 2000, ApJ, 544, 671
Werner, M. W., Roellig, T. L., Low, F. J., et al. 2004, ApJS, 154, 1
Willott, C. J., McLure, R. J., & Jarvis, M. J. 2003, ApJ, 587, L15